

RESEARCH ARTICLE | JANUARY 21 2022

# Lattice-plasmon-induced asymmetric transmission in two-dimensional chiral arrays

N. Apurv Chaitanya  ; M. A. T. Butt  ; O. Reshef  ; Robert W. Boyd  ; P. Banzer  ; Israel De Leon 



APL Photonics 7, 016105 (2022)

<https://doi.org/10.1063/5.0074849>



CrossMark

## Articles You May Be Interested In

Photosynthetic pigments of *Zoster a noltii* and *Ruppia cirrhosa* in some Albanian lagoons


*AIP Conference Proceedings* (January 2010)

Theory of the interaction of light with large inhomogeneous molecular aggregates. II. Psi-type circular dichroism

*J. Chem. Phys.* (March 1986)

Erratum: "Lattice-plasmon-induced asymmetric transmission in two-dimensional chiral arrays" [APL Photonics 7, 016105 (2022)]

*APL Photonics* (May 2022)



THE ADVANCED MATERIALS MANUFACTURER®

yttrium iron garnet    glassy carbon    beamsplitters    fused quartz    additive manufacturing

zeolites    III-IV semiconductors    gallium lump    copper nanoparticles    organometallics

nano ribbons    barium fluoride    europium phosphors    photonics    infrared dyes

sapphire windows    Nd:YAG    epitaxial crystal growth    ultra high purity materials    transparent ceramics    CIGS

spintronics    raman substrates    cerium oxide polishing powder    cermet    nanodispersions

silver nanoparticles    perovskites    surface functionalized nanoparticles    MBE grade materials    thin film

MOCVD    beta-barium borate    Osium    OLED lighting    solar energy

rare earth metals    quantum dots    sputtering targets    fiber optics

osmium    scintillation Ce:YAG    h-BN    deposition slugs

refractory metals    laser crystals    CVD precursors    photovoltaics

antiferromagnetic films    niobate    InAs wafers    metamaterials    borosilicate glass

25th Anniversary    MOFs    AuNPs    YBCO    superconductors    InGaAs

ZnS    CdTe    indium tin oxide    MgF2    rutile    optical glass

perovskite crystals    transparent ceramics    diamond micropowder

The Next Generation of Material Science Catalogs

**Now Invent.™**

[www.americanelements.com](http://www.americanelements.com)

© 2001-2022, American Elements is a U.S. Registered Trademark

# Lattice-plasmon-induced asymmetric transmission in two-dimensional chiral arrays

Cite as: APL Photon. 7, 016105 (2022); doi: 10.1063/5.0074849

Submitted: 11 October 2021 • Accepted: 3 January 2022 •

Published Online: 21 January 2022



N. Apurv Chaitanya,<sup>1</sup>  M. A. T. Butt,<sup>2,3,4,5</sup>  O. Reshef,<sup>6</sup>  Robert W. Boyd,<sup>5,6,7</sup>  P. Banzer,<sup>2,3,5,8</sup>   
and Israel De Leon<sup>1,5,9,a)</sup> 

## AFFILIATIONS

<sup>1</sup>Tecnologico de Monterrey, School of Engineering and Sciences, Ave. Eugenio Garza Sada 2501, Monterrey, Nuevo León 64849, Mexico

<sup>2</sup>Max Planck Institute for the Science of Light, Staudtstrasse 2, D-91058 Erlangen, Germany

<sup>3</sup>Institute of Optics, Information and Photonics, University Erlangen-Nuremberg, Staudtstrasse 7/B2, D-91058 Erlangen, Germany

<sup>4</sup>School in Advanced Optical Technologies, University Erlangen-Nuremberg, Paul-Gordan-Strasse 6, D-91052 Erlangen, Germany

<sup>5</sup>Max Planck, University of Ottawa Centre for Extreme and Quantum Photonics, University of Ottawa, Ottawa, Ontario K1N6N5, Canada

<sup>6</sup>Department of Physics, University of Ottawa, Ottawa, Ontario K1N 6N5, Canada

<sup>7</sup>The Institute of Optics, University of Rochester, Rochester, New York 14627, USA

<sup>8</sup>Institute of Physics, University of Graz, NAWI Graz, Universitätsplatz 5, 8010 Graz, Austria

<sup>9</sup>School of Electrical Engineering and Computer Science, University of Ottawa, Ottawa, Ontario K1N6N5, Canada

<sup>a)</sup>Author to whom correspondence should be addressed: [ideleon@tec.mx](mailto:ideleon@tec.mx)

## ABSTRACT

Asymmetric transmission—direction-selective electromagnetic transmission between two ports—is a phenomenon exhibited by two-dimensional chiral systems. The possibility of exploiting this phenomenon in chiral metasurfaces opens exciting possibilities for applications such as optical isolation and routing without external magnetic fields. This work investigates optical asymmetric transmission in chiral plasmonic metasurfaces supporting lattice plasmon modes and unveils its physical origins. We show numerically and experimentally that asymmetric transmission is caused by an unbalanced excitation of such lattice modes by circularly polarized light of opposite handedness. The excitation efficiencies of the lattice modes, and hence, the strength of the asymmetric transmission, are controlled by engineering the in-plane scattering of the individual plasmonic nanoparticles such that the maximum scattering imbalance occurs along one of the in-plane diffraction orders of the metasurface. Furthermore, we show that only the nonzero diffraction orders contribute to this effect. By highlighting the role of the localized plasmon modes supported by the nanoparticle and their radiative coupling to the lattice structure, our study provides a guideline for designing metasurfaces with asymmetric transmission enabled by lattice plasmons.

© 2022 Author(s). All article content, except where otherwise noted, is licensed under a Creative Commons Attribution (CC BY) license (<http://creativecommons.org/licenses/by/4.0/>). <https://doi.org/10.1063/5.0074849>

## I. INTRODUCTION

Chirality refers to an intrinsic sense of handedness of a three-dimensional (3D) structure, which remains invariant regardless of the direction of observation. Because of this property, the structure and its mirror image cannot be brought into congruence by a translation and rotation operation.<sup>1</sup> Proteins, chemical systems, and many biomolecules are known to be chiral, exhibiting

contrasting functions and properties between its mirror-symmetric pairs (enantiomer).<sup>2–4</sup> 3D chiral systems yield a different optical response when interacting with either handedness of circularly polarized light, leading to phenomena such as circular dichroism and optical activity. Both phenomena are widely used for characterizing the optical response of chiral systems.<sup>5</sup> Chirality could also be defined for two-dimensional (2D) structures. However, as planar structures do not possess an intrinsic handedness, chirality is defined

by the inability of a 2D structure and its mirror image to be brought into congruence unless lifted from its plane.<sup>6</sup> Systems composed of achiral structures are known to exhibit chiral effects, provided that the surface normal and the electric field vector form a chiral triad.<sup>6–8</sup> This phenomenon, usually called *extrinsic chirality*, is indistinguishable from standard (intrinsic) chirality<sup>9</sup> and has been reported in a variety of systems, including single nanoparticles.<sup>10,11</sup>

The sense of handedness of a 2D chiral structure is reversed when it is flipped with respect to an in-plane axis.<sup>9</sup> Because of this property, 2D chiral structures can show asymmetric optical transmission, i.e., for a given circular polarization state, the optical transmittance depends on the side of the sample that is being illuminated.<sup>12–15</sup> This is in compliance with the Lorentz reciprocity theorem and does not require magnetic fields as for the Faraday effect.<sup>12</sup> The phenomenon can also be observed as a difference in reflection and/or a difference in absorption. Occasionally, the term circular dichroism has been used to refer to asymmetric transmission. However, it is essential to note that circular dichroism is exclusive to 3D chiral systems, while asymmetric transmission is exclusive to 2D chiral systems. Although circular dichroism has been reported in 2D arrays through extrinsic chirality, the experimental geometry in such cases tends to the structure 3D chiral.<sup>6–8</sup> Another distinguishing feature of asymmetric transmission from circular dichroism is that the former changes the sign of the signal upon reversal of direction of illumination, whereas the latter remains invariant with respect to this operation.

Chiroptical phenomena have been extensively explored in plasmonic systems, such as individual nanostructures,<sup>16–19</sup> 2D array of plasmonic nanostructures (metasurfaces),<sup>20–23</sup> and plasmonic nanostructures in suspension (metafluids).<sup>24</sup> Of particular interest is the asymmetric transmission in chiral plasmonic metasurfaces. When the periodic interparticle spacing of such metasurfaces is smaller than the optical wavelength, the asymmetric transmission has been attributed to the simultaneous presence of anisotropy and losses.<sup>12,13,25</sup> However, when the interparticle spacing is of the order of the optical wavelength, the metasurface can support lattice plasmon modes enabled by diffractive coupling of localized plasmons,<sup>26,27</sup> which, in turn, can enable a different mechanism of asymmetric transmission. The asymmetric transmission of 2D chiral arrays supporting lattice plasmon modes has been reported recently;<sup>28,29</sup> however, the origin of this phenomenon remains unclear.

In this work, we unveil the physical origin of the lattice-plasmon-induced asymmetric transmission in diffractive chiral metasurfaces. Through a numerical and experimental analysis, we show that the asymmetric transmission mechanism relies on different lattice plasmon mode excitation efficiencies for left circularly polarized (LCP) and right circularly polarized (RCP) lights. Such excitation efficiencies can be controlled by tailoring the nanoparticle's in-plane distribution of scattered light for circularly polarized excitation and its alignment with the in-plane diffraction orders of the metasurface. Contrary to previous reports,<sup>29</sup> our study shows that the lattice-plasmon-induced asymmetric transmission results solely from the contribution of nonzero diffraction orders.

For simplicity, we analyze this phenomenon for a metasurface composed of an array of achiral nanoparticles—a *tetramer* consisting of four nanoantennas, as shown in the inset of Fig. 1.

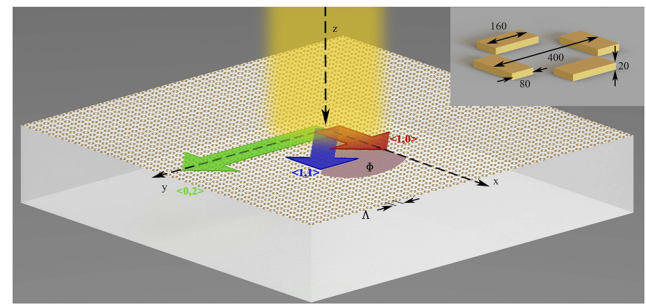


**FIG. 1.** Schematic illustration of the metasurfaces under investigation. The metasurface is illuminated at normal incidence by circularly polarized light propagating in the positive  $z$  direction. The metasurface consists of a square array of gold tetramers embedded in a homogeneous medium. The arrangement and dimensions of the four nanoantennas composing the tetramer are shown in the inset. All dimensions are given in nanometers.

We show that near the Rayleigh anomaly condition, where the asymmetric transmission effect is the strongest, the metasurface supports lattice plasmon modes that respond selectively to the polarization handedness, confirming the underlying asymmetric transmission mechanism enabled by the lattice plasmon modes. These results are of general relevance for understanding the role of diffracted waves in 2D chiral systems, particularly for the design of chiral plasmonic metasurfaces.

## II. ASYMMETRIC TRANSMISSION MECHANISM AND NUMERICAL ANALYSIS

Consider the metasurface depicted in Fig. 1, which consists of a planar array of tetramer nanostructures. The tetramers are made of gold, arranged into a squared lattice, and surrounded by a homogeneous medium with the refractive index  $n = 1.51$  (i.e., glass). The array lies on the  $(x$  and  $y)$  plane, having a lattice spacing  $\Lambda = 600$  nm. The dimensions of each tetramer are indicated in the inset of Fig. 1. The metasurface is illuminated by a circularly polarized plane wave propagating in the positive  $z$  direction and impinging at a normal incidence onto the surface. Although the individual tetramers are achiral, it is possible to create a 2D chiral metasurface by rotating the tetramer at each lattice point around its center.

The metasurface can support lattice plasmon modes when  $\Lambda$  is of the order of the optical wavelength. These modes result from the coupling of light scattered from neighboring particles through grazing diffraction orders or Rayleigh anomalies.<sup>26,30</sup> For a normally incident excitation, such Rayleigh anomalies occur at wavelengths given by<sup>31</sup>

$$\lambda_{p,q} = n\Lambda \frac{\sqrt{(p^2 + q^2) - q^2} \pm p}{p^2 + q^2}, \quad (1)$$

where  $p$  and  $q$  are the integers indicating the in-plane diffraction orders along the  $x$  and  $y$  directions, respectively. The Rayleigh anomaly condition for the first diffraction order,  $\langle p, q \rangle = \langle 0, 1 \rangle = \langle 1, 0 \rangle$ , is degenerate and occurs at the wavelength  $\lambda_{1,0} = 906$  nm. Similarly, the next Rayleigh anomaly, which corresponds to the diffraction order  $\langle 1, 1 \rangle$ , occurs at  $\lambda_{1,1} = 640$  nm. Lattice plasmon modes propagating along different in-plane  $\langle p, q \rangle$  diffraction orders

are supported at wavelengths close to those described by Eq. (1). The direction of the three main  $\langle p, q \rangle$  diffraction orders is depicted in Fig. 1.

To understand the asymmetric transmission mechanism exhibited by this metasurface, we first analyze the optical scattering properties of the individual tetramers for LCP and RCP plane-wave illumination. For this, we use a fully vectorial Maxwell equation solver based on the finite-difference time domain (FDTD) method.

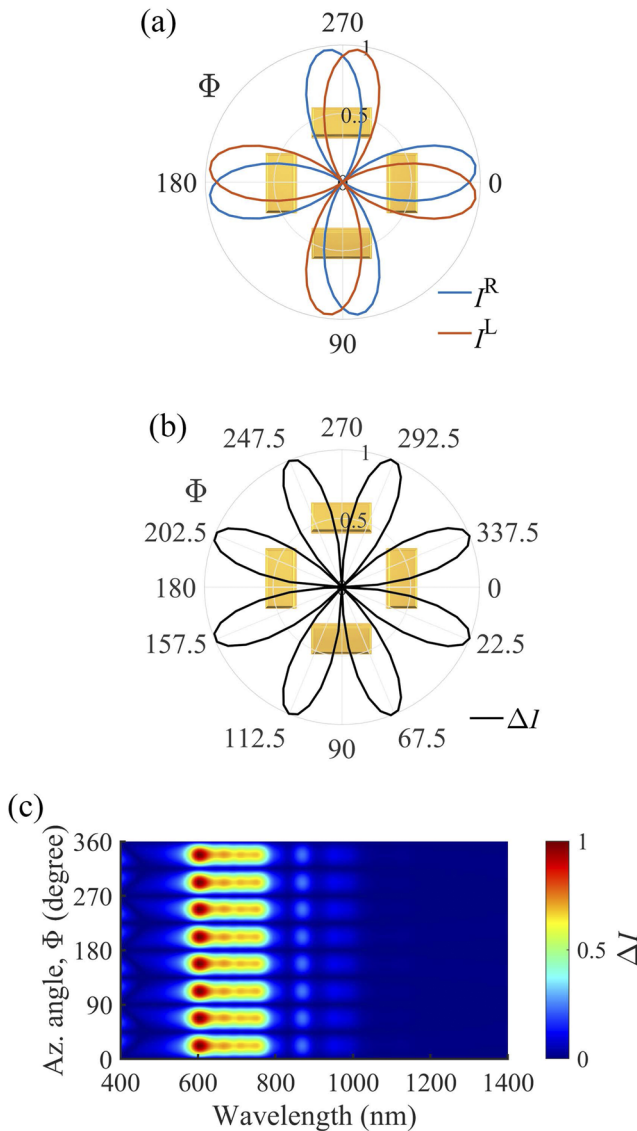


**FIG. 2.** Optical response of the isolated nanostructure obtained through FDTD simulations. (a) Polar plot of the far-field scattered intensity as a function of in-plane angle for an individual nanostructure.  $I^R$  and  $I^L$  are the normalized scattered intensity for RCP (solid blue) and LCP (solid red) excitations. (b) Normalized plots of differential in-plane scattering,  $\Delta I = |I^R - I^L|$ , for a 620 nm excitation wavelength. Superimposed on the plots is the isolated nanostructure for reference. (c) Variation in  $\Delta I$  as a function of wavelength for the nanostructure in normalized units.

The permittivity of gold was taken from Ref. 32. Figure 2(a) shows the obtained in-plane angular distribution of the scattered intensity at the wavelength  $\lambda = 620$  nm, which is close to the particle's resonance. Here,  $I^L$  and  $I^R$  are the in-plane scattered intensities for LCP and RCP excitations, respectively. The difference between these intensities,  $\Delta I = |I^R - I^L|$ , will be referred to as the differential in-plane scattering. This quantity is plotted in Fig. 2(b) for the same wavelength as Fig. 2(a) and as a function of wavelength in Fig. 2(c). Observe that regardless of the optical wavelength, the differential in-plane scattering has maxima ( $\Delta I_{\max}$ ) and minima ( $\Delta I_{\min}$ ) at particular azimuthal angles whose values are odd and even integer multiples of  $22.5^\circ$ , respectively.

The individual tetramer exhibits a nonzero differential in-plane scattering in a spectral range overlapping with the Rayleigh anomalies of the array. Consequently, the lattice plasmon excitation efficiency will vary depending on whether the tetramer array is illuminated with RCP or LCP light, leading to different transmittances for each case. In turn, this leads to asymmetric transmission, as reversing the polarization handedness is equivalent to illuminating the metasurface from the opposite side. Moreover, since  $\Delta I$  varies along the in-plane angle, the differential excitation of lattice plasmon modes by RCP and LCP lights also varies with the relative angle between  $\Delta I$  and the lattice plasmon mode propagation direction. In particular, when  $\Delta I_{\max}$  ( $\Delta I_{\min}$ ) is along the propagation direction of a lattice plasmon mode, the difference in the efficiency of excitation of that lattice plasmon mode will be maximized (minimized).

To analyze this effect, the transmittance of the metasurface as a function of tetramer's rotation angles is computed and plotted in Fig. 3(a) for RCP illumination; a similar result is obtained for LCP illumination (not shown). These transmittance results obtained for RCP and LCP illuminations will be used for estimating the asymmetric transmission. The relative orientation of the nanostructure for different rotation angles with respect to the lattice is illustrated in Figs. 3(c)–3(f). Figure 3(b) shows the asymmetric transmission calculated from the numerical results as

$$AT = \frac{T^R - T^L}{T^R + T^L}, \quad (2)$$

where  $T^R$  and  $T^L$  are the transmittance for RCP and LCP excitations, respectively. The asymmetric transmission vanishes for wavelengths beyond 906 nm because the Rayleigh anomaly condition is not satisfied, and so, the lattice plasmon modes are not supported. On the other hand, the asymmetric transmission is maximized at wavelengths close to the Rayleigh anomaly conditions ( $\lambda_{10}$  and  $\lambda_{11}$ ), where lattice plasmon modes are most efficiently excited.

Most importantly, we note that the asymmetric transmission depends on the in-plane rotation of the individual tetramers. Clearly, the largest asymmetric transmission is obtained when the individual nanostructure is rotated by odd integer multiples of  $22.5^\circ$ , which coincides with the angles for  $\Delta I_{\max}$  of the isolated nanostructure [see Fig. 2(b)]. The [supplementary material](#) gives a detailed analysis of the asymmetric transmission arising from an array of chiral nanostructures. From these results, we conclude that the value of the differential in-plane scattering of the individual nanostructure,  $\Delta I$ , along the diffraction orders at the Rayleigh anomaly condition determines the strength of the asymmetric transmission. Furthermore, we note that when lattice plasmon modes are excited,



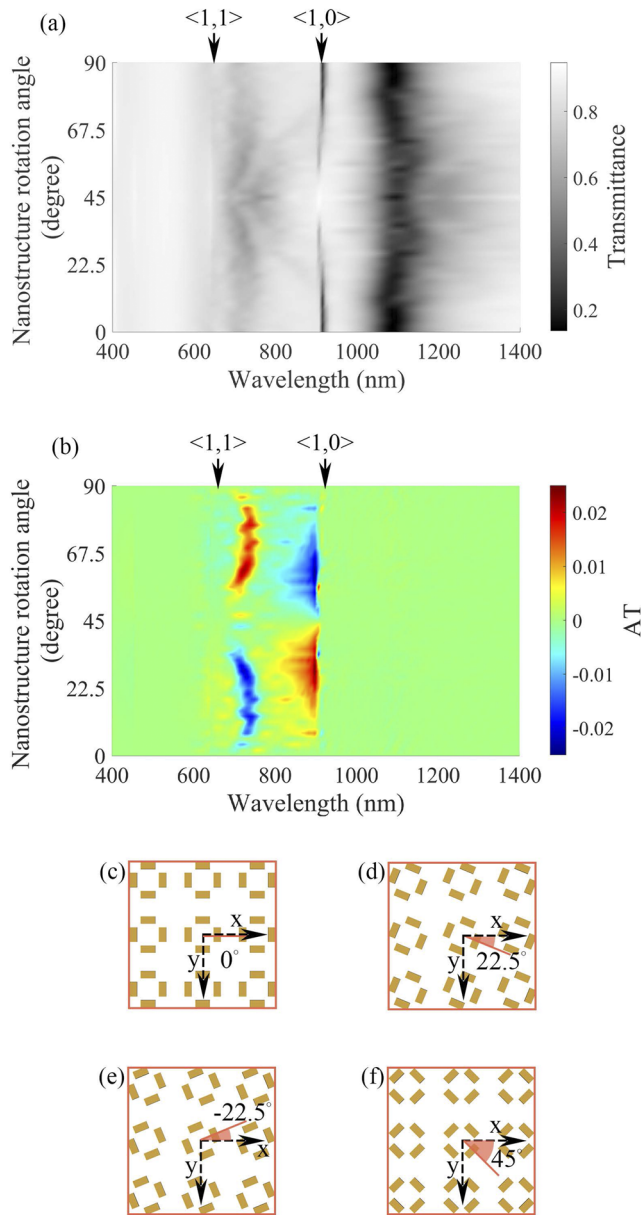


**FIG. 3.** (a) Numerically calculated transmittance spectra for RCP excitation for the metasurface as a function of rotation of the individual nanostructure. The arrows at the top of the results denote the wavelengths at which the Rayleigh anomalies occur, corresponding to a lattice period of  $\Lambda = 600$  nm in a homogeneous medium with  $n = 1.51$ . (b) Variation in asymmetric transmission calculated using Eq. (2) as a function of the tetramer's rotation angle. Asymmetric transmission occurs when the maxima of the differential in-plane scattering are aligned along the propagation direction of the grazing diffraction order. (c)–(f) show the schematic illustration of the metasurface when the individual nanostructure at each lattice point is rotated around its center.

the metasurface can exhibit asymmetric transmission as long as the individual nanostructure exhibits differential in-plane scattering along the lattice plasmon mode propagation direction. Hence, even for a nanostructure having fourfold rotational symmetry, the

presence of higher-order diffraction and the associated losses for the higher-orders can result in broken rotational symmetry of the entire process,<sup>33</sup> thereby making it irrelevant whether the nanostructure is chiral or achiral and whether it has fourfold rotational symmetry or not.

It is important to note here that isolated nanostructures exhibit differential in-plane scattering only when higher-order electric and magnetic moments are excited (see the [supplementary material](#)). Hence, there are three necessary conditions for asymmetric transmission in 2D chiral arrays composed of fourfold rotationally symmetric structures: (i) excitation of higher-order localized plasmonic resonances (resulting in-plane differential scattering), (ii) excitation of lattice plasmon modes, and (iii) an angular overlap between the maxima of in-plane differential scattering and the lattice plasmon mode propagation direction.

Finally, an analysis of the transmission characteristics for RCP and LCP excitations along different diffraction orders, away from the Rayleigh anomaly condition, reveals that the transmission into the zeroth-order is degenerate for both excitations irrespective of the wavelength and nanostructure rotation angles. Thus, the asymmetric transmission observed in Fig. 3(b) is caused solely by the difference in transmission of higher diffraction orders.

### III. EXPERIMENTAL RESULTS

Based on the numerical analysis, the fabrication of tetramer metasurfaces with the required orientation of individual structures was carried out. Details about the fabrication process can be found in the [supplementary material](#). A schematic illustration of the experimental setup used for the investigation is shown in Fig. 4(a). A filtered broadband light source is used to carry out spectrally resolved measurements in a range of 630–950 nm. A broadband polarizer followed by a quarter-wave-plate is used to prepare the polarization state of the excitation beam. The beam is then weakly focused to a diameter of  $\sim 50$   $\mu\text{m}$  with the help of a convex lens (effective NA  $\sim 0.015$ ), and the metasurface is precisely placed in the focal spot with the help of a three-axis piezo stage. A detailed description of the experimental setup can be found in the [supplementary material](#).

We consider three metasurfaces with in-plane rotation of nanostructures at  $22.5^\circ$ ,  $-22.5^\circ$ , and  $45^\circ$  to measure the lattice-plasmon-induced asymmetric transmission. For the present metasurface designs, a significant fraction of the transmitted power remains in the zeroth-order, hindering the experimental observations of the effect. Hence, we perform diffraction-resolved measurements to identify the independent power contributions of the transmitted zeroth and first diffraction orders. To this end, the transmitted light is collected with a microscope objective (NA = 1.3), with its back focal plane imaged onto a CCD camera. The back focal plane gives us access to the wave-vector space ( $k$ -space) of the transmitted light from which we obtain the diffraction-resolved power contributions (see the [supplementary material](#)). The zeroth-order is measured for all wavelengths. The first diffraction orders can be measured only for wavelengths shorter than 780 nm because of the limitation imposed by the maximum collection angle of the microscope objective ( $60.25^\circ$ ). This limitation prevents us from measuring the power coupled to lattice plasmon modes (near the Rayleigh anomaly wavelengths). For such cases, we employ direct

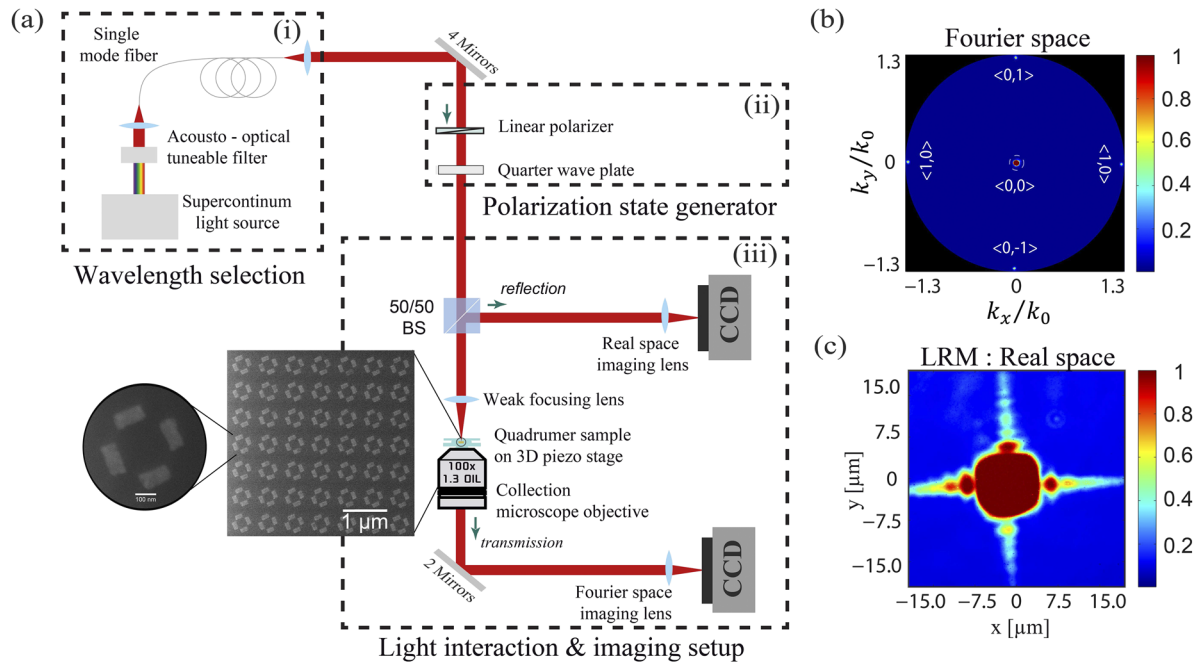


**FIG. 4.** (a) Sketch of the experimental setup. A broadband light source is filtered to perform spectrally resolved measurements. A broadband polarizer followed by a quarter-wave-plate is used to prepare the polarization state of the excitation beam. The beam is weakly focused ( $\text{NA} = 0.015$ ), producing a focal spot of  $\sim 50 \mu\text{m}$  diameter on the tetramer metasurface. The transmitted light is collected with a microscope objective of  $\text{NA} = 1.3$ . The objective's back focal plane, containing the  $k$ -space information, is imaged onto a CCD camera. (b) The  $k$ -space image recorded in transmission at an input wavelength of 770 nm. Zeroth and first diffraction orders are visible, which were evaluated for contributions to asymmetric transmission. (c) For direct imaging of the tetramer metasurface, in reflection, at Rayleigh anomaly, we adjust the incident illumination and use a microscope objective with effective  $\text{NA} = 0.1$  to illuminate and subsequently collect the reflected light.

imaging of the metasurface in reflection via leakage radiation microscopy. We adjust the incident illumination and use a microscope objective with effective  $\text{NA} = 0.1$  to illuminate and subsequently collect the reflected light. This objective selection in reflection consequently results in a focused spot size smaller than in the transmission case. The use of slightly higher  $\text{NA}$  for imaging in reflection helps in clearly observing the leaky propagating first diffraction orders, as shown in Fig. 4(c). This technique allows us to obtain qualitative information of the power coupled to lattice plasmon modes by visualizing light leaked as they propagate. Figures 4(b) and 4(c) illustrate, respectively,  $k$ -space and leakage radiation microscopy images recorded using the above mentioned techniques.

The experimental measurements of lattice-plasmon-induced asymmetric transmission obtained for the achiral ( $45^\circ$  rotation) and chiral ( $22.5^\circ$  and  $-22.5^\circ$  rotations) metasurfaces are summarized in Fig. 5. The diffraction-resolved asymmetric transmission for the zeroth and first diffraction orders is plotted in Fig. 5(a) as a function of the wavelength; both measurements (dashed lines) and simulations (solid lines) are included in the plots. Diffraction-resolved asymmetric transmission is calculated using Eq. (2), but  $T_R$  and  $T_L$  are replaced with  $T_R^{(p,q)}$  and  $T_L^{(p,q)}$ , which are the transmittance in the  $\langle p, q \rangle$  diffraction order for RCP and LCP excitations, respectively. Leakage radiation microscopy images are used to study the phenomenon at a wavelength close to the Rayleigh anomaly (marked by gray dashed line in spectral plots), by constructing

differential measurements obtained from a pixel-by-pixel subtraction of two camera shots taken for excitation with opposite polarization handedness. Such differential leakage radiation microscopy images, as shown in Fig. 5(b), allow us to visualize the asymmetric excitation of lattice plasmon modes responsible for the asymmetric transmission.

First, we discuss the case of the metasurface with tetramers rotated by  $45^\circ$  in-plane [see Fig. 5(a) top-left], which constitutes an achiral metasurface. As expected, this metasurface results in vanishing asymmetric transmission in first diffraction orders, which is confirmed by both experimental and simulation results. The differential leakage radiation microscopy image recorded for this metasurface also confirms vanishing asymmetric propagating modes [see Fig. 5(b), marked in green box]. Next, consider the metasurface constituted by tetramers with in-plane rotations of  $22.5^\circ$  and  $-22.5^\circ$  [see Fig. 5(a) top-center and top-right, respectively]. As expected from simulation results shown in Fig. 3(d), the two corresponding cases show opposing signs of asymmetric transmission for the first-order. This is confirmed by the experimental results, as shown in the spectral plot in Fig. 5(a). The differential leakage radiation microscopy image recorded for the chiral arrangements depicts asymmetrically excited lattice plasmon modes with opposing signs [see Fig. 5(b), marked in blue and red boxes].

To demonstrate and validate the sole contribution of the first diffraction orders to the observed asymmetric transmission, we

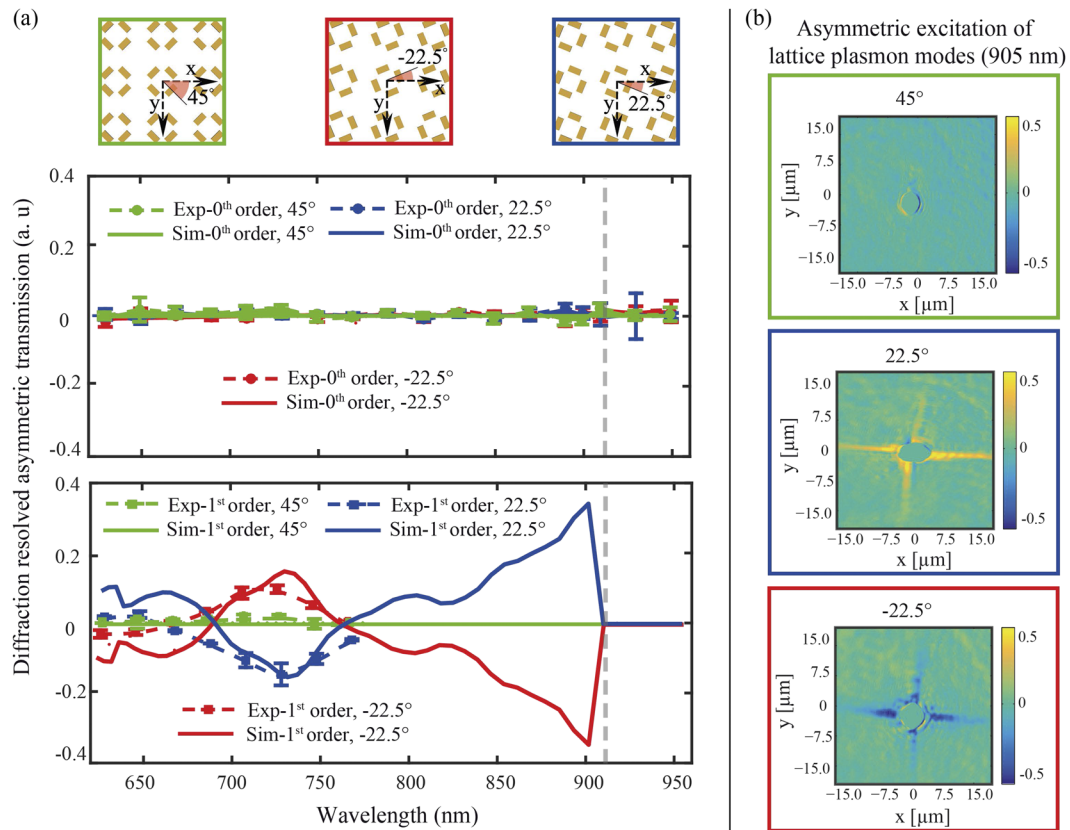


**FIG. 5.** Experimental and simulated diffraction-resolved asymmetric transmission results for achiral ( $45^\circ$  rotation) and chiral ( $22.5^\circ$ – $22.5^\circ$  rotations) metasurfaces. (a) Wavelength vs diffraction-resolved asymmetric transmission for zeroth (top panel) and first diffraction order (bottom panel) for the achiral (green) and chiral (blue and red) metasurfaces. (b) Differential leakage radiation microscopy (LRM) images recorded at 905 nm wavelength, showing asymmetric excitation of lattice plasmon modes for chiral ( $22.5^\circ$  and  $22.5^\circ$  rotations) metasurfaces with opposing signs and symmetric excitation of lattice plasmon modes for the achiral metasurface ( $45^\circ$ ).

also show the corresponding simulation and experimental results for the zeroth diffraction order not featuring any significant spectral dependence for all three studied metasurfaces [see Fig. 5(a) center]. The absence of asymmetric transmission for all three tetramer metasurfaces for the zeroth-order underscores the essential role of lattice plasmon modes in the asymmetric transmission mechanism.

#### IV. CONCLUSIONS

In conclusion, we studied the role of lattice plasmon modes on the phenomenon of asymmetric transmission in chiral 2D arrays of plasmonic nanoparticles and explained its physical origin. We showed that the difference in the nanoparticle's in-plane scattering of LCP and RCP lights can contribute to asymmetric transmission in 2D metasurfaces through the excitation of polarization-handedness selective lattice plasmon modes. The difference in the nanoparticle's in-plane scattering is attributed to the excitation of higher-order localized plasmonic resonances. The different excitation efficiencies

of the lattice plasmon modes, produced by unbalanced in-plane scattering of LCP and RCP lights and its coupling to grazing diffraction orders of the periodic lattice, result in asymmetries in transmission, reflection, and absorption. As the difference in the in-plane scattered intensity varies as a function of the in-plane angle around the nanostructure, rotating the nanostructure in the plane of the metasurface can act as a handle to control the metasurface's asymmetric transmission. Using diffraction-order-resolved transmission measurements, we demonstrated that the asymmetric transmission results solely from contributions of higher-order diffracted waves, while the zeroth-order transmission is not asymmetric. Furthermore, we showed that, even though the isolated nanostructure has a fourfold rotational symmetry, diffractive metasurfaces can exhibit asymmetric transmission for normal incidence illumination within the spectral range for which lattice plasmon modes are supported. This behavior is contrary to what occurs in a non-diffractive chiral metasurface. Our study sheds new light on asymmetric or chiral phenomena in metasurfaces and the critical role of diffraction effects such as the excitation of lattice plasmon modes.

## SUPPLEMENTARY MATERIAL

Details about the fabrication process, experimental setup, and analysis of the asymmetric transmission arising from gammadion metasurface can be found in the [supplementary material](#).

## ACKNOWLEDGMENTS

I.D.L. acknowledges the financial support from the Federico Baur Endowed Chair in Nanotechnology. R.W.B. acknowledges support from the Natural Sciences and Engineering Research Council of Canada, the Canada Research Chairs program, the U.S. ARO under Grant No. W911NF-18-1-0337, and U.S. DARPA under Award No. W911NF1810369.

## AUTHOR DECLARATIONS

### Conflict of Interest

The authors declare no conflicts of interest.

## DATA AVAILABILITY

The data that support the findings of this study are available within the article and its [supplementary material](#).

## REFERENCES

- G. H. Wagnière, *On Chirality and the Universal Asymmetry: Reflections on Image and Mirror Image* (John Wiley & Sons, 2008).
- M. F. Maestre, C. Bustamante, T. L. Hayes, J. A. Subirana, and I. Tinoco, "Differential scattering of circularly polarized light by the helical sperm head from the octopus *Eledone cirrhosa*," *Nature* **298**, 773 (1982).
- T. P. Yoon and E. N. Jacobsen, "Privileged chiral catalysts," *Science* **299**, 1691–1693 (2003).
- A. Pfaltz and W. J. Drury, "Design of chiral ligands for asymmetric catalysis: From C<sub>2</sub>-symmetric P,P- and N,N-ligands to sterically and electronically nonsymmetrical P,N-ligands," *Proc. Natl. Acad. Sci. U. S. A.* **101**, 5723–5726 (2004).
- N. Berova, K. Nakanishi, R. W. Woody, and R. Woody, *Circular Dichroism: Principles and Applications* (John Wiley & Sons, 2000).
- A. Papakostas, A. Potts, D. M. Bagnall, S. L. Prosvirnin, H. J. Coles, and N. I. Zheludev, "Optical manifestations of planar chirality," *Phys. Rev. Lett.* **90**, 107404 (2003).
- E. Plum, X. X. Liu, V. A. Fedotov, Y. Chen, D. P. Tsai, and N. I. Zheludev, "Metamaterials: Optical activity without chirality," *Phys. Rev. Lett.* **102**, 113902 (2009).
- I. De Leon, M. J. Horton, S. A. Schulz, J. Upham, P. Banzer, and R. W. Boyd, "Strong, spectrally-tunable chirality in diffractive metasurfaces," *Sci. Rep.* **5**, 13034 (2015).
- E. Plum, V. A. Fedotov, and N. I. Zheludev, "Extrinsic electromagnetic chirality in metamaterials," *J. Opt. A: Pure Appl. Opt.* **11**, 074009 (2009).
- X. Lu, J. Wu, Q. Zhu, J. Zhao, Q. Wang, L. Zhan, and W. Ni, "Circular dichroism from single plasmonic nanostructures with extrinsic chirality," *Nanoscale* **6**, 14244–14253 (2014).
- A. Yokoyama, M. Yoshida, A. Ishii, and Y. K. Kato, "Giant circular dichroism in individual carbon nanotubes induced by extrinsic chirality," *Phys. Rev. X* **4**, 011005 (2014).
- V. A. Fedotov, P. L. Mladyonov, S. L. Prosvirnin, A. V. Rogacheva, Y. Chen, and N. I. Zheludev, "Asymmetric propagation of electromagnetic waves through a planar chiral structure," *Phys. Rev. Lett.* **97**, 167401 (2006); [arXiv:0604234 \[physics\]](#).
- V. A. Fedotov, A. S. Schwanecke, N. I. Zheludev, V. V. Khardikov, and S. L. Prosvirnin, "Asymmetric transmission of light and enantiomerically sensitive plasmon resonance in planar chiral nanostructures," *Nano Lett.* **7**, 1996–1999 (2007).
- A. S. Schwanecke, V. A. Fedotov, V. V. Khardikov, S. L. Prosvirnin, Y. Chen, and N. I. Zheludev, "Nanostructured metal film with asymmetric optical transmission," *Nano Lett.* **8**, 2940–2943 (2008).
- T. Aba, Y. Qu, T. Wang, Y. Chen, H. Li, Y. Wang, Y. Bai, and Z. Zhang, "Tunable asymmetric transmission through tilted rectangular nanohole arrays in a square lattice," *Opt. Express* **26**, 1199 (2018).
- N. Meinzer, E. Hendry, and W. L. Barnes, "Probing the chiral nature of electromagnetic fields surrounding plasmonic nanostructures," *Phys. Rev. B* **88**, 041407 (2013).
- B. Hopkins, A. N. Poddubny, A. E. Miroschnichenko, and Y. S. Kivshar, "Circular dichroism induced by Fano resonances in planar chiral oligomers," *Laser Photonics Rev.* **10**, 137–146 (2016).
- P. Banzer, P. Woźniak, U. Mick, I. De Leon, and R. W. Boyd, "Chiral optical response of planar and symmetric nanotrimers enabled by heteromaterial selection," *Nat. Commun.* **7**, 13117 (2016).
- P. Woźniak, I. De Leon, K. Höflich, C. Haverkamp, S. Christiansen, G. Leuchs, and P. Banzer, "Chiroptical response of a single plasmonic nanohelix," *Opt. Express* **26**, 19275–19293 (2018).
- A. Drezet, C. Genet, J.-Y. Laluet, and T. W. Ebbesen, "Optical chirality without optical activity: How surface plasmons give a twist to light," *Opt. Express* **16**, 12559–12570 (2008).
- M. Schäferling, D. Dregely, M. Hentschel, and H. Giessen, "Tailoring enhanced optical chirality: Design principles for chiral plasmonic nanostructures," *Phys. Rev. X* **2**, 031010 (2012).
- V. K. Valev, J. J. Baumberg, C. Sibilia, and T. Verbiest, "Chirality and chiroptical effects in plasmonic nanostructures: Fundamentals, recent progress, and outlook," *Adv. Mater.* **25**, 2517–2534 (2013).
- S. Zu, Y. Bao, and Z. Fang, "Planar plasmonic chiral nanostructures," *Nanoscale* **8**, 3900–3905 (2016).
- R. Schreiber, N. Luong, Z. Fan, A. Kuzyk, P. C. Nickels, T. Zhang, D. M. Smith, B. Yurke, W. Kuang, A. O. Govorov *et al.*, "Chiral plasmonic DNA nanostructures with switchable circular dichroism," *Nat. Commun.* **4**, 2948 (2013).
- A. B. Khanikaev, N. Arju, Z. Fan, D. Purtseladze, F. Lu, J. Lee, P. Sarriugarte, M. Schnell, R. Hillenbrand, M. Belkin *et al.*, "Experimental demonstration of the microscopic origin of circular dichroism in two-dimensional metamaterials," *Nat. Commun.* **7**, 12045 (2016).
- V. G. Kravets, A. V. Kabashin, W. L. Barnes, and A. N. Grigorenko, "Plasmonic surface lattice resonances: A review of properties and applications," *Chem. Rev.* **118**, 5912–5951 (2018).
- M. S. Bin-Alam, O. Reshef, Y. Mamchur, M. Z. Alam, G. Carlow, J. Upham, B. T. Sullivan, J.-M. Ménard, M. J. Huttunen, R. W. Boyd *et al.*, "Ultra-high-Q resonances in plasmonic metasurfaces," *Nat. Commun.* **12**, 974 (2021).
- M. Cotrufo *et al.*, "Spin-dependent emission from arrays of planar chiral nanoantennas due to lattice and localized plasmon resonances," *ACS Nano* **10**, 3389–3397 (2016).
- F. Mattioli, G. Mazzeo, G. Longhi, S. Abbate, G. Pellegrini, E. Moggi, M. Celibrano, M. Finazzi, L. Duò, C. G. Zanchi, M. Tommasini, M. Pea, S. Cibella, R. Polito, F. Sciortino, L. Baldassarre, A. Nucara, M. Ortolani, and P. Biagioni, "Plasmonic superchiral lattice resonances in the mid-infrared," *ACS Photonics* **7**, 2676–2681 (2020).
- V. G. Kravets, F. Schedin, and A. N. Grigorenko, "Extremely narrow plasmon resonances based on diffraction coupling of localized plasmons in arrays of metallic nanoparticles," *Phys. Rev. Lett.* **101**, 087403 (2008).
- D. Khlopun, F. Laux, W. P. Wardley, J. Martin, G. A. Wurtz, J. Plain, N. Bonod, A. V. Zayats, W. Dickson, and D. Gérard, "Lattice modes and plasmonic linewidth engineering in gold and aluminum nanoparticle arrays," *J. Opt. Soc. Am. B* **34**, 691–700 (2017).
- P. B. Johnson and R. W. Christy, "Optical constants of the noble metals," *Phys. Rev. B* **6**, 4370 (1972); [arXiv:1011.1669v3](#).
- S. L. Prosvirnin and N. I. Zheludev, "Polarization effects in the diffraction of light by a planar chiral structure," *Phys. Rev. E* **71**, 037603 (2005).